High Temperatures-High Pressures, Vol. 48, pp. 367–380
Reprints available directly from the publisher
Photocopying permitted by license only
DOI: 10.32908/hthp.v48.691

High-pressure synthesis and thermal expansivity investigation of carbonate solid solutions $Mg_{1-x}Mn_xCO_3$

Rui Li[1,2], Wen Liang[1], Hanqi He[1,2], Yong Meng[3] and Hongfeng Tang[1,*]

[1]*Key Laboratory of High temperature and High pressure Study of the Earth's Interior, Institute of Geochemistry, Chinese Academy of Sciences, Guiyang, 550081, China*
[2]*University of Chinese Academy of Sciences, Beijing, 100049, China*
[3]*State Key Laboratory of Ore Deposit Geochemistry, Institute of Geochemistry, Chinese Academy of Sciences, Guiyang, 550081, China*

Received: April 16, 2018; Accepted: July 3, 2018.

Using synthesized $MgCO_3$ and reagent-grade $MnCO_3$ as starting materials, a series of $Mg_{1-x}Mn_xCO_3$ carbonate solid solutions were synthesized by a simple solid reaction under high-temperature-pressure conditions of 3 GPa and 800 °C for 4 h. The phase compositions of as-synthesized $Mg_{1-x}Mn_xCO_3$ samples were investigated by powder X-ray diffraction (XRD); no impurities were observed. The lattice parameters were refined and showed a linear relationship as a function of the Mn^{2+} content, which is expected to be in accordance with the ideal solution model. Based on this, high-temperature XRD measurements were carried out to further study the thermal expansivity of $Mg_{1-x}Mn_xCO_3$. The axis thermal expansion coefficients (α_a and α_c) and the volumetric thermal expansion coefficient α_V for $Mg_{1-x}Mn_xCO_3$ were quantified as $\alpha_a = 7.41 \times 10^{-6}$/°C, $\alpha_c = 2.37 \times 10^{-5}$/°C and $\alpha_V = 3.86 \times 10^{-5}$/°C for x = 0.0; $\alpha_a = 6.67 \times 10^{-6}$/°C, $\alpha_c = 2.31 \times 10^{-5}$/°C and $\alpha_V = 3.67 \times 10^{-5}$/°C for x = 0.1; $\alpha_a = 6.16 \times 10^{-6}$/°C, $\alpha_c = 2.35 \times 10^{-5}$/°C and $\alpha_V = 3.59 \times 10^{-5}$/°C for x = 0.3; $\alpha_a = 5.91 \times 10^{-6}$/°C, $\alpha_c = 2.40 \times 10^{-5}$/°C and $\alpha_V = 3.58 \times 10^{-5}$/°C for x = 0.5; $\alpha_a = 5.47 \times 10^{-6}$/°C, $\alpha_c = 2.53 \times 10^{-5}$/°C and $\alpha_V = 3.61 \times 10^{-5}$/°C for x = 0.7; $\alpha_a = 4.76 \times 10^{-6}$/°C, $\alpha_c = 2.55 \times 10^{-5}$/°C and $\alpha_V = 3.52 \times 10^{-5}$/°C for x = 0.9; $\alpha_a = 4.18 \times 10^{-6}$/°C, $\alpha_c = 2.50 \times 10^{-5}$/°C and $\alpha_V = 3.35 \times 10^{-5}$/°C for x = 1.0. The thermal expansion coefficients (α_a, α_c and α_V) can be fitted with a symmetric cubic function of the Mn^{2+} content as $\alpha_a = 7.34 \times 10^{-6} - 7.06 \times 10^{-6}x + 1.21 \times 10^{-5}x^2 - 8.19 \times 10^{-6}x^3$; $\alpha_c = 2.37 \times 10^{-6} - 7.94 \times 10^{-6}x + 2.57 \times 10^{-5}x^2 - 1.64 \times 10^{-5}x^3$; $\alpha_V = 3.85 \times 10^{-5} - 2.08 \times 10^{-5}x + 4.59 \times 10^{-5}x^2 - 3.01 \times 10^{-5}x^3$.

* Corresponding author: tanghongfeng@vip.gyig.ac.cn

Keywords: carbonate solid solution $Mg_{1-x}Mn_xCO_3$, high-temperature XRD, thermal expansion coefficient

1 INTRODUCTION

Carbonates with various compositions are widely distributed in the Earth and participate in the chemistry and dynamics of many geological processes [1]. Recently, interest in carbonates has grown significantly given that the global carbon cycle has been a subject of great concern in geosciences [2–4]. Investigation of the physical and chemical properties of carbonates is necessary for greater understanding of the global carbon cycle and carbon storage [5,6].

Understanding of thermal stability and thermal expansion properties of carbonates is of vital significance for the study of the P-V-T equation of state (EoS), which is highly important for capturing the existence of carbon storage from the Earth's surface to the interior. In the past few decades, a large amount of research on EoS of carbonates has been performed using in-situ synchrotron XRD or high-temperature XRD (Here, XRD is the abbreviation of X-ray diffraction, which is widely used for determining the information about lattice morphology of atoms or molecules), leading to significant gains in the understanding of the thermal properties of carbonates [7–10]. However, natural carbonates have been used as the object of study in most previous work as a result of the unavailability of high purity synthetic samples. Because of the unavoidable adverse impacts of impurities, this could reduce the reliability of experimental results. Thus, it is rather difficult to systematically study the thermal expansion properties, and the quantified relationship between the thermal expansivity and the composition of carbonates remains unclear.

Considering that natural carbonates are mainly complex $CaCO_3$-$MgCO_3$-$FeCO_3$-$MnCO_3$ solid solutions, model binary, ternary and quaternary carbonates are necessary for all quantitative research on carbonate minerals [11]. Previous reports have solved the problem of the synthesis of impurity-free $MgCO_3$ and $FeCO_3$ [12–15], and thus, all impurity-free end member carbonates, including $CaCO_3$, $MgCO_3$, $FeCO_3$, and $MnCO_3$, are available for material science. Subsequently, impurity-free binary-join carbonates can be synthesized directly through a solid solution reaction from certain end member carbonates, which establishes an ideal clean material model for scientific research on carbonate minerals.

In this paper, solid solutions of $Mg_{1-x}Mn_xCO_3$ were selected as a binary-join model of carbonates in order to study thermal expansion properties. A series of carbonate $Mg_{1-x}Mn_xCO_3$ were synthesized with continuous variation in solid solubility x. XRD characterization revealed that solid solutions of $Mg_{1-x}Mn_xCO_3$ belong to the ideal solution model. On this basis, thermal expansivity

was investigated using high-temperature XRD, and the thermal expansion coefficients of $Mg_{1-x}Mn_xCO_3$, with various compositions x, was achieved.

2 EXPERIMENTS

$MgCO_3$ used as the starting material in our experiments was prepared using the high-pressure dehydration method reported by Liang *et al.* [14]: using $MgCO_3{\cdot}3H_2O$, anhydrous $MgCO_3$ was synthesized at 3 GPa and 800 °C for 1h. The starting materials $MgCO_3$ and $MnCO_3$ (99.99%, Alfa Aesar) were mixed to form the composition $Mg_{1-x}Mn_xCO_3$ (x ranging from 0.1 to 0.9) and then ground in an agate mortar with acetone. The sample pellet was created and sealed into a silver capsule of 4 mm diameter and 3 mm length. Using h-BN as the pressure medium, high-pressure synthesis was performed in an end-loaded piston-cylinder apparatus (LPC250–300/50, Max Voggenreiter GmbH, Germany) at 3 GPa and 800°C for 4 h; the temperature was then quenched to room temperature within 1min and the pressure was released slowly. The sample was obtained after removing the silver capsule. The pressure of the piston-cylinder was calibrated by quartz - coesite phase transition at 3 GPa [16]. A graphite heater (6 mm inner diameter and 8 mm outer diameter) and K-type thermocouple were used in these experiments.

In the thermal analysis process, Thermogravimetric (TG) analysis and Differential Scanning Calorimeter (DSC) were determined by a simultaneous thermal analyzer (STA 449F3, NETZSCH, Germany). The sample (20 mg) was heated from 40°C (5°C/min heating rate) in an argon atmosphere. High-temperature XRD data of as-synthesized $Mg_{1-x}Mn_xCO_3$ was obtained below its decomposition temperature using a Panalytical multifunction X-ray diffractometer (model: Empyrean), equipped with an Anton Paar high-temperature accessory (APHTK-16N). The heating process was carried out from ambient temperature to 400°C with an increase of 40°C per step in argon atmosphere. Every high-temperature step was maintained for 10 minutes to ensure temperature uniformity, and 10 XRD patterns were recorded for every series of solid solution $Mg_{1-x}Mn_xCO_3$.

The value of thermal expansion coefficients closely depends on the data fitting process of high-temperature XRD. For this reason, Peakfit + UnitCell software, given the importance of data accuracy, was used to refine the structure parameters [17]. It uses a direct solution algorithm from the Bragg equation and has better accuracy because it avoids the impacts of refinement parameters and functions. All diffraction peaks were fit with Gaussian + Lorentzian functions by Peakfit software to quantify diffraction angles for every high-temperature XRD pattern, in which the goodness of fit was given by R^2. The position of the diffraction peaks with corresponding hkl were then input into UnitCell software, and the unit cell

parameters (a, c, and unit cell volume) from the high-temperature XRD data collected from 25°C to 400°C were then calculated.

3 RESULTS AND DISCUSSION

3.1 The synthesis of $Mg_{1-x}Mn_xCO_3$ solid solutions and powder XRD

A previous study reported that $MgCO_3$ and $MnCO_3$ carbonates should form complete solid solutions [18], and our results confirm these findings. $Mg_{1-x}Mn_xCO_3$ solid solutions were obtained by solid reaction from pure $MgCO_3$ and $MnCO_3$, and analyzed by powder XRD in the step scan mode, as given in Figure 1(a). Figure 1(a) shows that all the diffraction peaks can be indexed as calcite-type rhombohedral structure without any impurity peaks. With increasing Mn^{2+} content, all peaks shifted obviously to lower angles because of expansion of the unit cell resulting from the substitution of Mg^{2+} by the much larger Mn^{2+}. Moreover, systematic changes in intensity were also observed; the intensity of (012) peaks increased with increasing Mn^{2+} content, while on the contrary, the intensity of (006) peaks deceased, which is very similar to the results from $Mg_{1-x}Fe_xCO_3$ solid solutions [19].

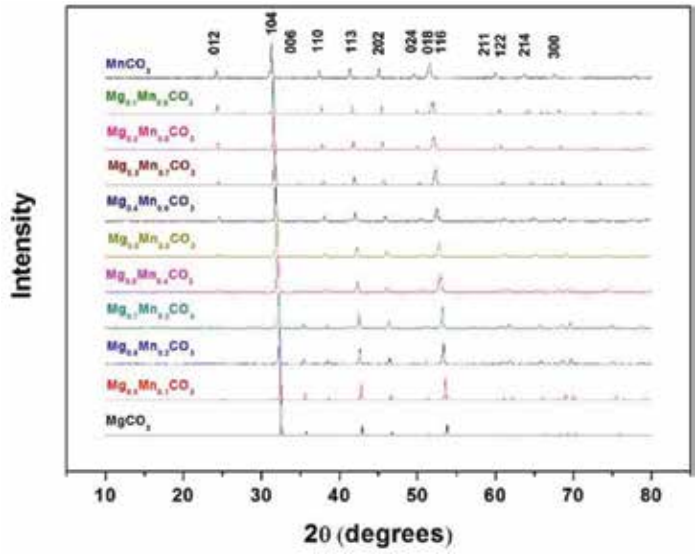

FIGURE 1 (a)
The relative intensity of XRD pattern of $Mg_{1-x}Mn_xCO_3$ solid solutions.

Furthermore, the lattice parameters of $Mg_{1-x}Mn_xCO_3$ solid solutions were refined by Peakfit and Unitcell software. The results are listed in Table 1 and shown in Figure 1(b)(c). The lattice parameters show a linear and continuous

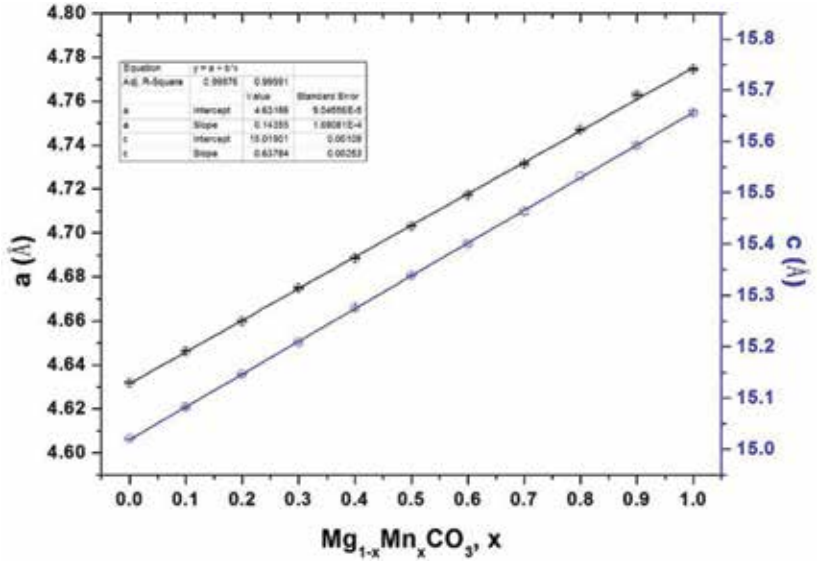

FIGURE 1 (b)
The relationship between the lattice parameters (a and c) of $Mg_{1-x}Mn_xCO_3$ solid solutions and Mn^{2+} content x.

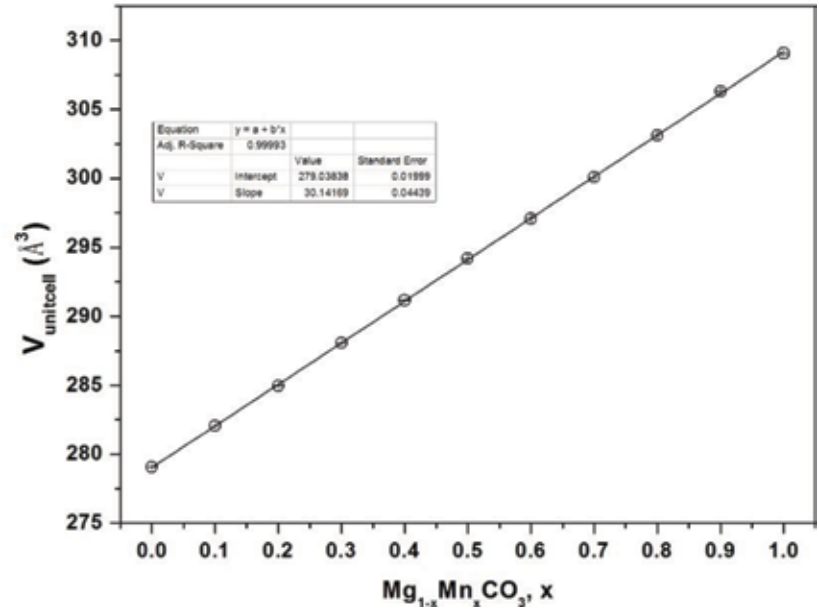

FIGURE 1 (c)
The relationship between the unit cell volume of $Mg_{1-x}Mn_xCO_3$ solid solutions and Mn^{2+} content x.

TABLE 1
The result of the lattice parameters of $Mg_{1-x}Mn_xCO_3$ solid solutions refined from XRD dates at various Mn^{2+} content x, where σa, σc and σV is the error bar of the parameters a, c and V, and R^2 is the goodness of fit given by Peakfit software.

x	a(Å)	σa(Å)	c(Å)	σc(Å)	V(Å^3)	σV(Å^3)	R^2
0.0	4.63196	0.00015	15.01983	0.00174	279.0781	0.0323	0.996857
0.1	4.64635	0.00016	15.08167	0.00177	282.0421	0.0333	0.993160
0.2	4.66002	0.00016	15.14674	0.00179	284.9684	0.0339	0.989024
0.3	4.67503	0.00016	15.20851	0.00178	288.0812	0.0336	0.982452
0.4	4.68851	0.00016	15.27613	0.00181	291.1459	0.0342	0.991445
0.5	4.70305	0.00019	15.33893	0.00184	294.1739	0.0349	0.986884
0.6	4.71728	0.00020	15.40007	0.00282	297.0703	0.0445	0.995874
0.7	4.73136	0.00020	15.46284	0.00368	300.0667	0.0610	0.995981
0.8	4.74693	0.00020	15.53318	0.00381	303.1215	0.0641	0.996248
0.9	4.76271	0.00020	15.59214	0.00379	306.3252	0.0637	0.989839
1.0	4.77453	0.00020	15.65562	0.00378	309.0739	0.0639	0.993056

increase with increasing temperature; the linear relationship can be fitted as follows:

$$a(x) = 4.63166 + 1.44 \times 10^{-1}x$$

$$c(x) = 15.01901 + 6.38 \times 10^{-1}x$$

$$V(x) = 279.038+30.142x$$

Figure 1(b)(c) show that $Mg_{1-x}Mn_xCO_3$ solid solutions obey the ideal solution model; that is, the lattice parameters are linearly dependent on Mn^{2+} content or Mn^{2+} solid solubility, which is the basis for systematic research of thermal expansion properties.

3.2 Thermal stability of $Mg_{1-x}Mn_xCO_3$ solid solutions at ambient conditions

Figure 2(a) shows the TG and DSC analysis of one end member, $MnCO_3$, which uses the argon atmosphere to protect the Mn^{2+} with a rate of temperature rise of 5°C/min. It can be seen clearly from the TG that a decomposition reaction occurs from 500°C to 640°C, which is higher than that of the end member $MgCO_3$ (from 420°C to 600°C) [14]. The final TG content was stabilized at about 66.8%, and the final decomposition product was identified as Mn_2O_3 by XRD, shown Figure 2(b); it indicates that the theoretical decomposition product MnO is so sensitive to oxygen fugacity that it cannot stabilize in an argon atmosphere [20]. Further, a strong endothermic peak at around 600°C was observed from DSC; the quantity of endothermic disintegration Q can be calculated as follows:

$$Q = \int_{500^\circ c}^{640^\circ c} DSC(t)dt = 24.11 \text{ KJ/mol}$$

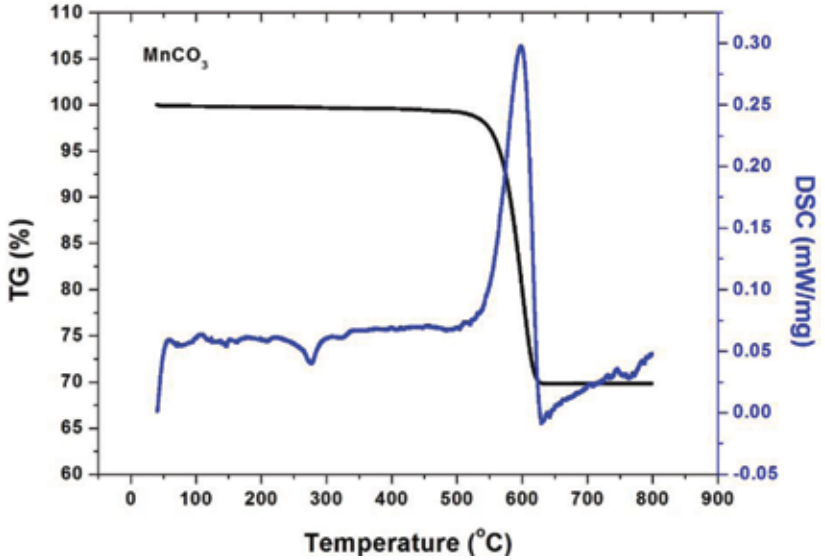

FIGURE 2 (a)
TG and DSC curves of $MnCO_3$

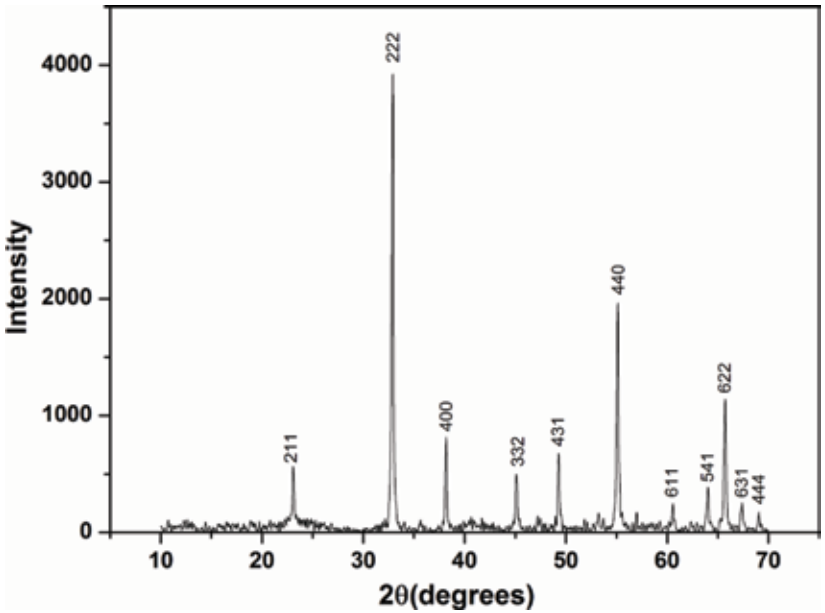

FIGURE 2 (b)
XRD pattern of final product from $MnCO_3$ TG, identified as Mn_2O_3

In accordance with the TG results of the two end members $MgCO_3$ and $MnCO_3$, the decomposition temperature of $Mg_{1-x}Mn_xCO_3$ solid solutions is expected to be higher than that of $MgCO_3$, and for this reason, the high-temperature XRD measurement of $Mg_{1-x}Mn_xCO_3$ could be carried out below 400°C.

3.3 The anisotropic coefficient of thermal expansion along a-axis and c-axis

The high-temperature XRD experiments for $Mg_{1-x}Mn_xCO_3$ solid solutions at x = 0.0, 0.1, 0.3, 0.5, 0.7, 0.9 and 1.0 were carried out below the expected decomposition temperature. The lattice parameters (a, c, cell volume) were refined by Peakfit and Unitcell software, and the correlations between the lattice parameters and temperature are given in Supplementary Table (a)–(g) and shown in Supplementary Figure (a)–(g), respectively. The lattice parameters show a linear and continuous increase with increasing temperature; the linear relationship can be fitted as follows,

For $MgCO_3$,

$$a(T) = 4.63082(1 + 7.41 \times 10^{-6}T),\ \alpha_a = 7.41 \times 10^{-6}/°C$$
$$c(T) = 15.00952(1 + 2.37 \times 10^{-5}T),\ \alpha_c = 2.37 \times 10^{-5}/°C$$
$$V(T) = 278.747(1 + 3.86 \times 10^{-5}T),\ \alpha_V = 3.86 \times 10^{-5}/°C$$

For $Mg_{0.9}Mn_{0.1}CO_3$,

$$a(T) = 4.64531(1 + 6.67 \times 10^{-6}T),\ \alpha_a = 6.67 \times 10^{-6}/°C$$
$$c(T) = 15.07110(1 + 2.31 \times 10^{-5}T),\ \alpha_c = 2.31 \times 10^{-5}/°C$$
$$V(T) = 281.714(1 + 3.67 \times 10^{-5}T),\ \alpha_V = 3.67 \times 10^{-5}/°C$$

For $Mg_{0.7}Mn_{0.3}CO_3$,

$$a(T) = 4.67395(1 + 6.16 \times 10^{-6}T),\ \alpha_a = 6.16 \times 10^{-6}/°C$$
$$c(T) = 15.19804(1 + 2.35 \times 10^{-5}T),\ \alpha_c = 2.35 \times 10^{-5}/°C$$
$$V(T) = 287.763(1 + 3.59 \times 10^{-5}T),\ \alpha_V = 3.59 \times 10^{-5}/°C$$

For $Mg_{0.5}Mn_{0.5}CO_3$,

$$a(T) = 4.70208(1 + 5.91 \times 10^{-6}T),\ \alpha_a = 5.91 \times 10^{-6}/°C$$
$$c(T) = 15.32834(1 + 2.40 \times 10^{-5}T),\ \alpha_c = 2.40 \times 10^{-5}/°C$$
$$V(T) = 293.848(1 + 3.58 \times 10^{-5}T),\ \alpha_V = 3.58 \times 10^{-5}/°C$$

For $Mg_{0.3}Mn_{0.7}CO_3$,

$$a(T) = 4.73092(1 + 5.47 \times 10^{-6}T),\ \alpha_a = 5.47 \times 10^{-6}/°C$$
$$c(T) = 15.45234(1 + 2.53 \times 10^{-5}T),\ \alpha_c = 2.53 \times 10^{-5}/°C$$
$$V(T) = 299.759(1 + 3.61 \times 10^{-5}T),\ \alpha_V = 3.61 \times 10^{-5}/°C$$

For $Mg_{0.1}Mn_{0.9}CO_3$,

$$a(T) = 4.76201(1 + 4.76 \times 10^{-6}T),\ \alpha_a = 4.76 \times 10^{-6}/°C$$
$$c(T) = 15.57725(1 + 2.55 \times 10^{-5}T),\ \alpha_c = 2.55 \times 10^{-5}/°C$$
$$V(T) = 305.940(1 + 3.52 \times 10^{-5}T),\ \alpha_V = 3.52 \times 10^{-5}/°C$$

For $MnCO_3$,

$$a(T) = 4.77380(1 + 4.18 \times 10^{-6}T),\ \alpha_a = 4.18 \times 10^{-6}/°C$$
$$c(T) = 15.64034(1 + 2.50 \times 10^{-5}T),\ \alpha_c = 2.50 \times 10^{-5}/°C$$
$$V(T) = 308.676(1 + 3.35 \times 10^{-5}T),\ \alpha_V = 3.35 \times 10^{-5}/°C$$

The thermal expansion coefficient α is quantified by the ratio (K/P_0) of the slope (K) to the intercept (P_0) in fitting the linear relationship, shown in Table 2, whereas the error bar of the thermal expansion coefficient is given by the differential relation $\sigma a = \sigma K / P_0 - (\frac{K}{P_0^2})\sigma P_0 \approx \sigma K / P_0$. The calculation of the axial thermal expansion coefficient and the approximate relation $\alpha_V \approx 2\alpha_a + \alpha_c$ for the rhombohedral structure is observed. The axial thermal expansivity exhibits obvious anisotropy: the c-axis thermal expansion coefficient of $MgCO_3$ ($\alpha_c = 2.37 \times 10^{-5}/°C$) is over three times greater than the a-axis ($\alpha_a = 7.41 \times 10^{-6}/°C$), which is in agreement with previous studies [7] [9] [14]. The c-axis thermal expansion coefficient of $MnCO_3$ ($\alpha_c = 2.50 \times 10^{-5}/°C$) is almost six times greater than the a-axis ($\alpha_a = 4.18 \times 10^{-6}/°C$), which may be related to the influence of bond length-bond angle behavior of more twisted (MnO_6) octahedral geometry. It was also observed that a-axis thermal expansion decreases while c-axis thermal expansion increases with increasing Mn^{2+} content. One possible reason is that, given the much longer (MgMn)-O bond length with increasing Mn^{2+} content, stretching through thermal expansion is more difficult, and the a-axis thermal expansion is consistent with that of the (MgMn)-O bond; with increasing Mn content, the increasing thermal expansion along the c-axis may be caused by distortion of the ($(MgMn)O_6$) octahedral geometry induced by the substitution of Mn^{2+}. Further support for this explanation requires more precise structural data obtained through high-temperature single crystal XRD.

TABLE 2
The thermal expansion coefficient of $Mg_{1-x}Mn_xCO_3$ solid solutions fitted by high- temperature XRD for various Mn^{2+} content x, in which α_a is the thermal expansion coefficient along a-axis, α_c is the thermal expansion coefficient along c-axis, α_V is the volumetric thermal expansion coefficient, and $\sigma\alpha_a$, $\sigma\alpha_c$ and $\sigma\alpha_V$ **is** the error bar of α_a, α_c and α_V, whereas the value of the error bar ($\sigma\alpha_a$, $\sigma\alpha_c$ and $\sigma\alpha_V$) is given by the approximative differential relation $\sigma\alpha \approx \sigma K/P_0$. The anisotropy of axial thermal expansion coefficient is given by α_c/α_a.

x	$\alpha_a \times 10^{-6}$ (/°C)	$\sigma\alpha_a \times 10^{-7}$ (/°C)	$\alpha_c \times 10^{-5}$ (/°C)	$\sigma\alpha_c \times 10^{-7}$ (/°C)	$\alpha_V \times 10^{-5}$ (/°C)	$\sigma\alpha_V \times 10^{-7}$ (/°C)	α_c/α_a
0.0	7.41	1.18	2.37	2.05	3.86	4.43	3.198
0.1	6.67	1.03	2.31	2.26	3.67	4.28	3.463
0.3	6.16	2.34	2.35	4.64	3.59	6.51	3.815
0.5	5.91	1.47	2.40	2.54	3.58	5.33	4.061
0.7	5.47	1.24	2.53	5.90	3.61	3.09	4.625
0.9	4.76	0.82	2.55	5.23	3.52	6.73	5.357
1.0	4.18	1.00	2.50	4.23	3.35	5.86	5.981

3.4 Investigation of thermal expansivity of $Mg_{1-x}Mn_xCO_3$ solid solutions

The results of the thermal expansion coefficients of $Mg_{1-x}Mn_xCO_3$ solid solutions (α_a, α_c, and α_V) corresponding to Mn^{2+} content x are listed in Table 2 and given in Figure 3(a)–(c), respectively. Thermal expansion coefficients were nonlinearly related to the continuous Mn^{2+} content, and can be fitted by a cubic function as follows:

$$\alpha_a = 7.34 \times 10^{-6} - 7.06 \times 10^{-6}x + 1.21 \times 10^{-5}x^2 - 8.19 \times 10^{-6}x^3$$

$$\alpha_c = 2.37 \times 10^{-5} - 7.94 \times 10^{-6}x + 2.57 \times 10^{-5}x^2 - 1.64 \times 10^{-5}x^3$$

$$\alpha_V = 3.85 \times 10^{-5} - 2.08 \times 10^{-5}x + 4.59 \times 10^{-5}x^2 - 3.01 \times 10^{-5}x^3$$

The red dashed line, which was used to connect two end members, is defined as baseline $\alpha_0(x)$, and the thermal expansion coefficient can be written as $\alpha(x) = \alpha_0(x) + \Delta\alpha(x)$, where $\Delta\alpha(x)$ is the modulation terms. We found that $\Delta\alpha(x)$ is regularly distributed on both sides of $\alpha_0(x)$, and exhibits centrosymmetry as an inversion center located at around x = 0.5. A symmetrical nonlinear law of thermal expansion coefficient α as a function of composition x was achieved: when x is less than 0.5, the disturbing term $\Delta\alpha(x)$ is negative and experimental measurement of $\alpha(x)$ is less than baseline $\alpha_0(x)$; conversely, when the composition is closed to end of $MnCO_3$, $\alpha(x)$ is greater than baseline $\alpha_0(x)$. This result may be related to the mechanism of Mg/Mn substitution in the rhombohedral crystal structure of carbonates.

The difference in Shannon effective ionic radii of Mn^{2+} and Fe^{2+} is very small, and therefore, $Mg_{1-x}Mn_xCO_3$ and $Mg_{1-x}Fe_xCO_3$ solid solutions are comparable in terms of thermal expansivity. By comparison, Merlini *et al.* reported the thermal expansion coefficient $\alpha(x)$ in the $MgCO_3$-$FeCO_3$

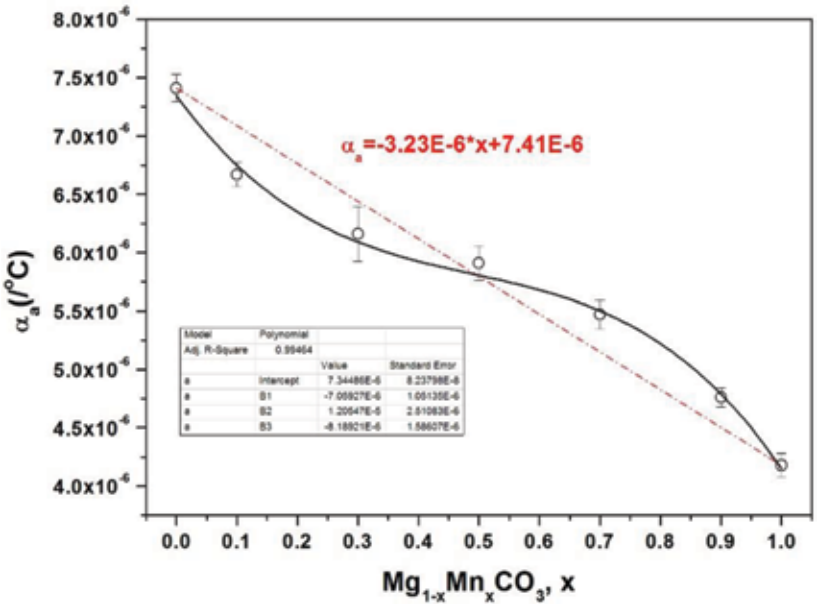

FIGURE 3 (a)
The thermal expansion coefficient along a-axis α_a as a function of various Mn^{2+} content x.

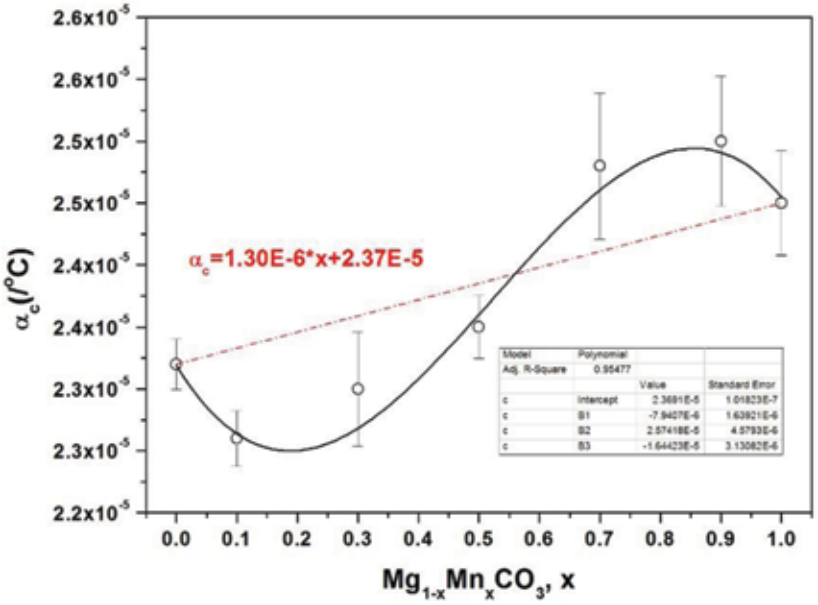

FIGURE 3 (b)
The thermal expansion coefficient along c-axis α_c as a function of various Mn^{2+} content x.

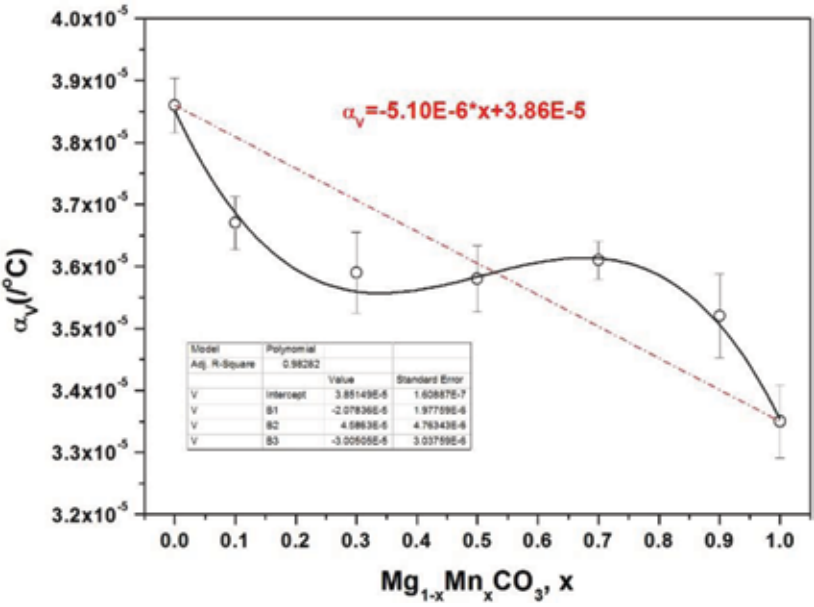

FIGURE 3 (c)
The volumetric thermal expansion coefficient α_V as a function of various Mn^{2+} content x.

binary-join natural carbonate [21], and a similar deviation from the baseline $\alpha_0(x)$ was also found. However, an important issue is that their conclusion $\Delta\alpha(x)$ is a little different from to our result. When the composition is closed to end of $MgCO_3$ ($x < 0.5$), the value of $\alpha(x)$ is greater than baseline $\alpha_0(x)$; when the composition is closed to end of $FeCO_3$ ($x > 0.5$), the value of $\alpha(x)$ is less than baseline $\alpha_0(x)$. This difference may be caused by the interference of Ca^{2+} and Mn^{2+} impurities in the natural carbonates used in the prior study.

4 CONCLUSION

A series of carbonate solid solutions of $Mg_{1-x}Mn_xCO_3$ were synthesized to design a binary-join model of carbonates for the investigation of thermal expansion. The thermal expansivity α as a function of Mn^{2+} content x was studied systematically, and a nonlinear law of thermal expansion coefficient α was determined. This could provide an experimental reference for thermodynamic calculation in carbonates. Further explanation of this nonlinear law is expected to provide more accurate single crystal structural data and theoretical calculation models.

ACKNOWLEDGEMENTS

We thank Yuan Yin, Zeming Li and Xiqiang Liu for technical assistance in Peakfit and Unitcell software. This work was financially supported by National Natural Science Foundation of China (Grant Number 41472065).

REFERENCES

[1] E.H. Oelkers, D.R. Cole, Carbon Dioxide Sequestration A Solution to a Global Problem, Elements, 4 (2008) 305–310. doi: 10.2113/gselements.4.5.305.

[2] K.D. Litasov, E. Ohtani, Solidus and phase relations of carbonated peridotite in the system $CaO–Al_2O_3–MgO–SiO_2–Na_2O–CO_2$ to the lower mantle depths, Physics of the Earth and Planetary Interiors, 177 (2009) 46–58. doi: 10.1016/j.pepi.2009.07.008.

[3] R. Dasgupta, M.M. Hirschmann, The deep carbon cycle and melting in Earth's interior, Earth and Planetary Science Letters, 298 (2010) 1–13. doi: 10.1016/j.epsl.2010.06.039.

[4] R.M. Hazen, R.J. Hemley, A.J. Mangum, Carbon in Earth's interior: storage, cycling, and life, Eos Transactions American Geophysical Union, 93 (2012) 17–18. doi: 10.1029/2012 EO020001.

[5] M. Isshiki, T. Irifune, K. Hirose, S. Ono, Y. Ohishi, T. Watanuki, E. Nishibori, M. Takata, M. Sakata, Stability of magnesite and its high-pressure form in the lowermost mantle, Nature, 427 (2004) 60–63. doi: 10.1038/nature02181.

[6] V. Stagno, Y. Tange, N. Miyajima, C.A. McCammon, T. Irifune, D.J. Frost, The stability of magnesite in the transition zone and the lower mantle as function of oxygen fugacity, Geophysical Research Letters, 38 (2011) 570–583. doi: 10.1029/2011GL049560.

[7] S.A. Markgraf, R.J. Reeder, High-temperature structure refinements of calcite and magnesite, American Mineralogist, 70 (1985) 590–600.

[8] J. Zhang, I. Martinez, F. Guyot, R. Reeder, Effects of Mg-Fe^{2+} substitution in calcite-structure carbonates: Thermoelastic properties, American Mineralogist, 83 (1998) 280–287. doi: 10.2138/am-1998-3-411. doi: 10.2138/am-1998-3-411.

[9] K.D. Litasov, Y. Fei, E. Ohtani, T. Kuribayashi, K. Funakoshi, Thermal equation of state of magnesite to 32GPa and 2073K, Physics of the Earth and Planetary Interiors, 168 (2008) 191–203. doi: 10.1016/j.pepi.2008.06.018.

[10] N. Floquet, D. Vielzeuf, D. Ferry, A. Ricolleau, V. Heresanu, J. Perrin, D. Laporte, A.N. Fitch, Thermally Induced Modifications and Phase Transformations of Red Coral Mg-Calcite Skeletons from Infrared Spectroscopy and High Resolution Synchrotron Powder Diffraction Analyses, Crystal Growth & Design, 15 (2015) 3690–3706. doi: 10.1021/acs.cgd.5b00291.

[11] E. Franzolin, M.W. Schmidt, S. Poli, Ternary Ca–Fe–Mg carbonates: subsolidus phase relations at 3.5 GPa and a thermodynamic solid solution model including order/disorder, Contributions to Mineralogy & Petrology, 161 (2011) 213–227. doi:10.1007/s00410-010-0527-x.

[12] B.M. French, Stability relations of siderite ($FeCO_3$) in the system Fe-C-O. American Journal of Science, 27 (1971) 37–78. doi: 10.2475/ajs.271.1.37.

[13] V. Cerantola, C. McCammon, I. Kupenko, I. Kantor, C. Marini, M. Wilke, L. Ismailova, N. Solopova, A. Chumakov, S. Pascarelli, L. Dubrovinsky, High-pressure spectroscopic study of siderite ($FeCO_3$) with a focus on spin crossover, American Mineralogist, 100 (2015) 2670–2681. doi: 10.2138/am-2015-5319.

[14] W. Liang, Y. Yin, L. Wang, L. Chen, H. Li, A new method of preparing anhydrous magnesium carbonate ($MgCO_3$) under high pressure and its thermal property, Journal of Alloys and Compounds, 702 (2017) 346–351. doi: 10.1016/j.jallcom.2017.01.258.

[15] W. Liang, Z. Li, Y. Yin, R. Li, L. Chen, Y. He, H. Dong, L. Dai, H. Li, Single crystal growth, characterization and high-pressure Raman spectroscopy of impurity-free magnesite ($MgCO_3$), Physics and Chemistry of Minerals, (2017). doi: 10.1007/s00269-017-0930-1.

[16] K. Bose, J. Ganguly, Quartz-coesite transition revisited: Reversed experimental determination at 500–1200ºC and retrieved thermochemical properties, American Mineralogist, 80 (1995) 231–238. doi: https://doi.org/10.2138/am-1995-3-405
[17] T.J.B. Holland, S.A.T. Redfern, Unit cell refinement from powder diffraction data: the use of regression diagnostics, Mineralogical Magazine, 61(1997) 65–77. doi: 10.1180/minmag.1997.061.404.07
[18] P.E. Rosenberg, Synthetic solid solutions in the systems $MgCO_3$-$FeCO_3$ and $MnCO_3$-$FeCO_3$, American Mineralogist, 48 (1963) 1396–1400.
[19] L. Chai, A. Navrotsky, Synthesis, characterization, and enthalpy of mixing of the (Fe, Mg) $C0_3$ solid solution, Geochimica et Cosmochimica Acta, 60 (1996) 4377–4383. doi: 10.1016/S0016-7037(96)00261-X.
[20] L.S. Capizzi, P. Fumagalli, S. Poli, S. Tumiati, The mobility of hydrous carbonate liquids in the mantle: an experimental model, Congresso Simp-sgi-sogei-aiv, 35 (2015) 122. doi: 10.13140/RG.2.1.3488.1760
[21] M. Merlini, F. Sapelli, P. Fumagalli, G.D. Gatta, P. Lotti, S. Tumiati, M. Abdellatief, A. Lausi, J. Plaisier, M. Hanfland, W. Crichton, J. Chantel, J. Guignard, C. Meneghini, A. Pavese, S. Poli, High-temperature and high-pressure behavior of carbonates in the ternary diagram $CaCO_3$-$MgCO_3$-$FeCO_3$, American Mineralogist, 101 (2016) 1423–1430. doi: 10.2138/am-2016-5458.